We are IntechOpen, the world's leading publisher of Open Access books Built by scientists, for scientists

6,900
Open access books available

185,000
International authors and editors

200M
Downloads

154
Countries delivered to

Our authors are among the

TOP 1%
most cited scientists

12.2%
Contributors from top 500 universities

CLARIVATE ANALYTICS
BOOK CITATION INDEX
INDEXED

WEB OF SCIENCE™

Selection of our books indexed in the Book Citation Index
in Web of Science™ Core Collection (BKCI)

Interested in publishing with us?
Contact book.department@intechopen.com

Advanced Multitemporal Phase Unwrapping Techniques for DInSAR Analyses

Antonio Pepe

Istituto per il Rilevamento Elettromagnetico dell'Ambiente (IREA),
Research National Council (CNR)
Italy

1. Introduction

Differential Synthetic Aperture Radar Interferometry (DInSAR) represents nowadays a well-established remote sensing technique to generate spatially dense surface deformation maps of large areas on Earth (Massonnet & Feigl, 1999; Bürgmann et. al., 2000). To achieve this task, the phase difference (known as interferogram) between SAR data pairs related to temporally-separated observations is exploited, retrieving a measure of the ground displacement projection along the radar line of sight (LOS) with centimeter to millimeter accuracy (Gabriel et. al., 1989).

Altough DinSAR methodology was originally applied to analyze single deformation episodes (Massonnet et. al., 1993; Goldstein et. a., 1993; Massonnet et. al., 1995; Peltzer et. al., 1995), it has recently applied with success to investigate the temporal evolution of the detected deformation phenomena through the generation of displacement time-series (Ferretti et. al., 2001; Berardino et. al., 2002) . In this case, the analysis is based on the computation of deformation time-series via the inversion of a properly chosen set of interferograms, produced from a sequence of temporally-separated SAR acquisitions relevant to the investigated area. In this context, two main categories of advanced DInSAR techniques for deformation time-series generation have been proposed in literature, often referred to as Persistent Scatterers (PS) (Ferretti et al., 2001; Hooper et. al., 2004), and Small Baseline (SB) (Berardino et. al., 2002; Mora et. al., 2003) techniques, respectively. The PS algorithms select all the interferometric data pairs with reference to a single common master image, without any constraint on the temporal and spatial separation (baseline) among the orbits. In this case, the analysis is carried out at the full resolution spatial scale, and is focused on the pixels containing a single dominant scatterer thus ensuring very limited temporal and spatial decorrelation phenomena (Zebker & Villasenor, 1992). Instead, for what concerns the SB techniques, the interferograms are generated by considering multiple master images, because this allows having interferometric data pairs with small temporal and spatial baselines. Accordingly, distributed targets can be also investigated, and the analysis may exploit both single-look and multi-look interferograms. Within the SB framework, a popular approach is the one referred to as Small BAseline Subset (SBAS), which was originally developed for analyzing multi-look interferograms (Berardino et. al., 2002) and subsequently adapted to the full resolution ones; in the latter case the low

resolution results are properly extended to the full resolution scale, as discussed in (Lanari et. al., 2004).

Despite the differences among the various implementations of the PS and SB algorithms, which are outside the scope of this work, a common problem to be faced is the Phase Unwrapping (PhU) operation representing the retrieval process of the full phase signals from their (measured) modulo-2π restricted components, often referred to as "interferometric fringes". In the context of the advanced DInSAR techniques, the need of jointly analyzing sequences of multi-temporal interferograms has more recently promoted the development of new PhU approaches with improved performances with respect to those focused on processing single interferograms. In this chapter, following the description of the basic rationale of the most widely used PhU techniques, we present a short review of the most recent space-time PhU methodologies with a particular emphasis on the Extended Minimum Cost Flow (EMCF) and its recent improvements. Some experimental results obtained by applying these latter approaches will be shown to demonstrate the validity of the presented algorithms.

2. Phase unwrapping

We start by introducing the key ideas at the base of most of the Phase Unwrapping (PhU) techniques proposed up to now in literature. As stated before, the phase unwrapping problem concerns the retrieval of the full interferometric phase (unwrapped ones) from its computed modulo-2π restricted components. Within DInSAR processing codes, PhU operation actually represents one the most critical task to be successfully accomplished. The problem in reconstructing the true phase from the measured one arises in the presence of aliasing errors mainly caused by the phase noise caused by low coherence and undersampling phenomena due to locally high fringe rates (related to the deformation signals associated to the interferograms).

To clarify the key aspects of the phase unwrapping problem, let us firstly focus on the problem to unwrap single interferograms. To this aim, let $\phi(a_z, r_g)$ be the interferometric phase measured in correspondence to the pixel of SAR coordinates (a_z, r_g). The unwrapping problem can be stated as the searching of the multiple 2π-integer that must be added to the wrapped phases to retrieve the full interferometric phase $\psi(a_z, r_g)$. Indeed:

$$\psi(a_z, r_g) = \phi(a_z, r_g) + 2\pi H(a_z, r_g) \tag{1}$$

This represents an ill-posed problem admitting an infinite set of acceptable solutions that can benefit from the knowledge of external information. In the absence of such information, the unwrapped field is typically reconstructed by computing the phase spatial gradients and integrating them over a "consistent" path. Accordingly, PhU algorithms can be grouped in two main categories depending on the fact that the unwrapping solution is path-dependent or not. To efficiently solve the problem, it is convenient to represent it in terms of discrete coordinates (x, y) being:

$$\begin{aligned} a_z &= a_{z0} + x\Delta a \\ r_g &= r_{g0} + y\Delta r \end{aligned} \tag{2}$$

wherein Δa and Δr are the azimuth and range pixel spacing, respectively and a_{z0} and r_{g0} the corresponding azimuth and range first lines. The discrete counterpart of the partial derivatives are then computed by using the popular wrapped-differences-of-wrapped-phases estimator $\langle \Delta\varphi \rangle_{-\pi,\pi} = arctg\left(\sin(\Delta\varphi)/\cos(\Delta\varphi)\right)$. Accordingly, the phase gradient vector can be defined as follows:

$$\hat{\nabla}\boldsymbol{\psi} = \langle \Delta_x\psi \rangle_{-\pi,\pi}\,\hat{\mathbf{x}} + \langle \Delta_y\psi \rangle_{-\pi,\pi}\,\hat{\mathbf{y}} \tag{3}$$

whose components with respect to the two spatial axis $\hat{x}$ and $\hat{y}$ are:

$$
\begin{aligned}
\langle \Delta_x\psi(x,y) \rangle_{-\pi,\pi} &= \langle \psi(x+1,y) - \psi(x,y) \rangle_{-\pi,\pi} = \langle \phi(x+1,y) - \phi(x,y) \rangle_{-\pi,\pi} \\
\langle \Delta_y\psi(x,y) \rangle_{-\pi,\pi} &= \langle \psi(x,y+1) - \psi(x,y) \rangle_{-\pi,\pi} = \langle \phi(x,y+1) - \phi(x,y) \rangle_{-\pi,\pi}
\end{aligned}
\tag{4}
$$

Accordingly, the phase gradient vector is estimated by wrapping possible phase differences greater than +/-π in the $[-\pi,\pi]$ interval by adding the correct multiples of 2π and by implicitly assuming that, in a properly sampled interferogram, the phase differences of adjacent samples are likely to be restricted to the $[-\pi,\pi]$ interval. Moreover, the probability that the phase difference exceed $\pm\pi$ depends both on the noise level (i.e. the lower is the coherence value the more likely the derivatives exceed $\pm\pi$). For this reason, the introduced operator is not conservative, that is:

$$rot\left(\hat{\nabla}\psi\right) = \nabla \times \left(\hat{\nabla}\psi\right) \neq 0 \tag{5}$$

Consequently, the integration of such phase gradients depends on the chosen integration path. This suggests us that a way to unwrap interferograms is to correct the phase gradients in such a way that the unwrapped phase can be recovered independently of the integration direction. Moreover, we can observe that the phase gradient estimate has the advantage that its errors are localized and come in integer multiples of 2π so that its curl (hereafter referred to as residue field) can be profitably used to reconstruct the full phase terms. The residue field expression (see Figure 1) is the following:

$$
\begin{aligned}
r(x,y) &= \nabla \times \left(\hat{\nabla}\psi(x,y)\right) = \Delta_x\left[\langle \Delta_y\psi(x,y) \rangle_{-\pi,\pi}\right] - \Delta_y\left[\langle \Delta_x\psi(x,y) \rangle_{-\pi,\pi}\right] = \\
&= \langle \Delta_x\psi(x,y) \rangle_{-\pi,\pi} + \langle \Delta_y\psi(x+1,y) \rangle_{-\pi,\pi} - \langle \Delta_x\psi(x,y+1) \rangle_{-\pi,\pi} - \langle \Delta_y\psi(x,y) \rangle_{-\pi,\pi}
\end{aligned}
\tag{6}
$$

Its values are either zero (no residues) or +/- 2π (positive or negative residue, respectively). Therefore, the goal of the phase unwrapping procedure is to eliminate potential integration paths enclosing unequal numbers of positive and negative residues. Residue derives from two sources in the radar measurements. The former is related to the true discontinuities in the data: the fringe spacing may be so fine on certain topographic slopes or, from large inter-observation displacement, such to exceed the Nyquist criterion of half-cycle spacing. The latter is the noise present in the data set, whatever from thermal and other noise sources or from decorrelation due to baseline length and temporal changes in the scene. However, residues from whatever source require compensation in the phase unwrapping procedure.

One of the major PhU algorithm exploits the fact that residues mark the endpoints of lines in the interferogram along which the true phase gradient exceed π/sample, these lines are commonly referred to as "branch-cuts" or "ghost-lines". Most of the algorithm up to now proposed are based on a proper compensation of these residues and, among these, we will concentrate in the following on the residue-cut and the least-square approaches (Zebker & Lu, 1998).
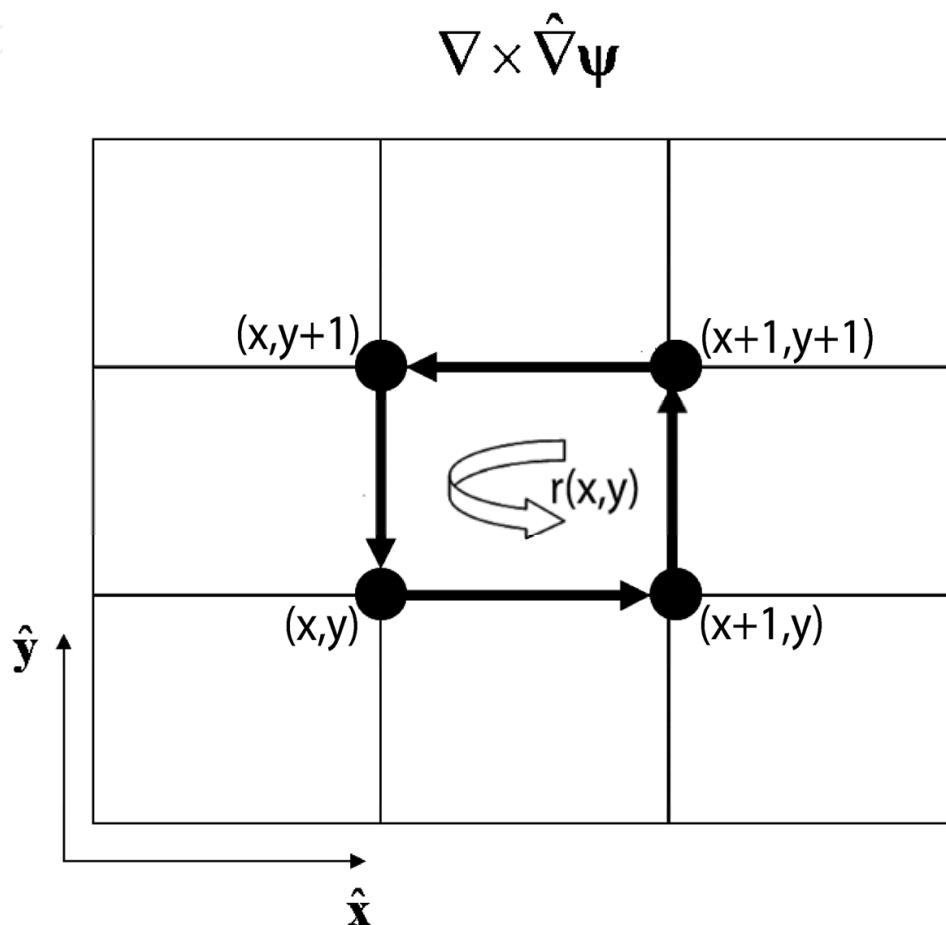

Fig. 1. Representation of the residue field.

2.1 Branch-cut algorithms

Within this class of algorithms we will point out our interest in particular on the so-called "residue-cut tree algorithm". The initial residue-cut phase unwrapping procedure proposed in (Golstein et. al., 1998) is implemented by first of all identifying the locations of all residues in an interferogram, and then connecting them with branch-cuts, so as to prevent the existence of integration paths that can encircle unbalanced numbers of positive and negative residues. The tree algorithm is a relatively conservative algorithm that tends to grow rather dense networks of trees in residue-rich regions. The algorithm initially connects closely spaced, oppositely charged, pairs of residues with cuts that prevent integration paths between them and, if all permitted integration paths enclose equal numbers of positive and negative residues, the consistency is assured. Progressively longer trees are permitted until all residues are connected to, at least one, other residue and until the next charge on each

tree is zero. Networks on small trees are used to prevent any single branch from becoming too long and isolating large sub-areas from the rest of the image. A consequence of the indiscriminate branch growth until charge neutrality is achieved from all trees, and all residues accounted for, is that in residue-rich regions the tree growth is so dense that the region is isolated from the remainder of the image and no unwrapped phase estimate can be obtained. By concluding, this conservative approach nearly eliminates mistakes but, at the expense of providing an incomplete unwrapping result.

2.2 Least-squares algorithms

The second major class of Phase Unwrapping algorithms, commonly in use today, was presented by (Ghiglia & Romero, 1994), who applied a mathematical formalism first developed by Hunt [69] to the radar interferometry phase unwrapping problem. Hunt developed a matrix formulation suitable for general phase reconstruction problems; Ghiglia found that a discrete cosine transform technique permits accurate and efficient least-squares inversion, even for the very large matrices encountered in the radar interferometry special case. In particular, the un-weighted LS method performs the following minimization problem

$$\min_{\tilde{\boldsymbol{\psi}}} \left\{ \sum_i \sum_j \left| \nabla \tilde{\boldsymbol{\psi}}(x,y) - \hat{\nabla} \boldsymbol{\psi}(x,y) \right|^2 \right\} \tag{7}$$

where $\tilde{\boldsymbol{\psi}}$ is the unknown unwrapped phase field. We may stress that, with respect to the branch-cut approaches, in these cases the solution will be no longer congruent with the original interferometric phase.

Equation (7) represents a variational problem, whose Euler equation is the Poisson one:

$$\nabla^2 \tilde{\psi}(x,y) = \nabla \cdot \nabla \tilde{\psi}(x,y) = \Delta_x \left(\langle \Delta_x \psi(x,y) \rangle_{-\pi,\pi} \right) + \Delta_y \left(\langle \Delta_y \psi(x,y) \rangle_{-\pi,\pi} \right) \tag{8}$$

under the Neumann boundary condition, which can be finally solved by using simple cosine or Fourier transform filtering (Fornaro et. al., 1996).

One major difference between the residue-cut and least-squares solutions is that in the residue-cut approach only integral numbers of cycles are added to the measurements to produce the result. Conversely, in the least-squares approach, any value may be added to ensure smoothness and continuity in the solution, thus the spatial error distribution may differ between the approaches, and the relative merits of each method must be determined depending on the application.

Least-squares methods are very computationally efficient when they make use of fast Fourier transform techniques but the resulting unwrapping is not very accurate, because they tend to spread the errors instead of concentrating them on a limited set of points. To overcome this problem a weighting of the wrapped phase can be useful. However, the proposed, weighted least squares algorithms are iterative and not as efficient as the un-weighted ones, and the result accuracy strongly depends on the used weighting mask.

Several other approaches, which can be found in the bibliography at the end of this work, have also been investigated but, in the following, we will address the capability of one of these, known as the minimum cost flow phase unwrapping technique, developed for the two-dimensional case by (Costantini, 1998), and belonging to the branch-cuts PhU algorithm class.

2.3 Minimum cost flow algorithms

Within the branch-cuts phase unwrapping algorithms an easy and fast algorithm is based on a solution of an equivalent minimum cost flow network and will be here addressed.

Branch-cut methods are based on the integration of the estimated neighbouring pixel differences of the unwrapped phase along conservative paths, thus avoiding the regions where these estimated differences are inconsistent. The problem of building cuts delimiting these regions is very difficult and the resulting phase unwrapping algorithm is very computationally expensive. However, we may exploit the fact that the neighbouring pixel differences of the unwrapped phases are estimated with possibly an error that is an integer multiple of 2π. This circumstance allows the formulation of the phase unwrapping problem as the one of minimizing the weighted deviations between the estimated and the unknown neighbouring pixel differences of the unwrapped phases with the constraint that the deviations must be integer multiple of 2π. With this constraint, the unwrapping results will not depend critically on the weighting mask we used, and errors are prevented to spread.

Minimization problems with integer variables are usually computationally very complex. However, recognizing the network structure underlying the phase unwrapping problem, it makes possible to employ very efficient strategies for its solution. In fact, the problem can be equated to the one of finding the minimum cost flow on a network, for the solution of which there are very efficient algorithms. To explain its basic principles and clarify how it can be performed, we refer to the unknown, unwrapped phase field and we impose that the result is consistent, thus requiring the irrotational property of this field:

$$
\begin{aligned}
\nabla \times \nabla \psi(x,y) &= \Delta_x\left(\Delta_y\psi(x,y)\right) - \Delta_y\left(\Delta_x\psi(x,y)\right) = \\
&= \Delta_x\psi(x,y) + \Delta_y\psi(x+1,y) - \Delta_x\psi(x,y+1) - \Delta_y\psi(x,y) = 0
\end{aligned}
\tag{9}
$$

Obviously, we can also express each term of (9) with respect to the wrapped phase derivates by introducing, for each phase term, a corresponding, unknown 2π-multiple term, as follows:

$$
\begin{aligned}
\Delta_x\psi(x,y) &= \left\langle \Delta_x\psi(x,y) \right\rangle_{-\pi,\pi} + 2\pi K_x(x,y) \\
\Delta_y\psi(x+1,y) &= \left\langle \Delta_y\psi(x+1,y) \right\rangle_{-\pi,\pi} + 2\pi K_y(x+1,y) \\
\Delta_x\psi(x,y+1) &= \left\langle \Delta_x\psi(x,y+1) \right\rangle_{-\pi,\pi} + 2\pi K_x(x,y+1) \\
\Delta_y\psi(x,y) &= \left\langle \Delta_y\psi(x,y) \right\rangle_{-\pi,\pi} + 2\pi K_y(x,y)
\end{aligned}
\tag{10}
$$

These relations eventually lead to the following equation

$$K_x(x,y) + K_y(x+1,y) - K_x(x,y+1) - K_y(x,y) = -\frac{r(x,y)}{2\pi} \tag{11}$$

that relates the integer unknowns to the measurable residues. At this stage, the phase unwrapping problem can be formulated as the searching of the K terms that satisfy the constraints (11) and solve the following minimization problem:

$$\min_{K_x K_y} \left\{ \sum_x \sum_y c_x(x,y)|K_x(x,y)| + \sum_x \sum_y c_y(x,y)|K_y(x,y)| \right\} \tag{12}$$

being c( ) the so-called cost functions allowing us to individuate areas where the location of branch-cuts is likely or unlikely. It is easy to verify that, whether the costs were chosen constant, the problem (12) would be equivalent to search for the minimum total cut-line length. Cost functions are essentially expressed as a function of the estimated local interferogram quality (by exploiting the spatial coherence, or the phase gradient density or other properly identified quality factors). The problem given in (12) is a non-linear minimization problem with integer variables, and, if the following change of variables is considered

$$\begin{aligned}
K_x^-(x,y) &= \min\left[0, K_x(x,y)\right] \\
K_x^+(x,y) &= \max\left[0, K_x(x,y)\right] \\
K_y^-(x,y) &= \min\left[0, K_y(x,y)\right] \\
K_y^+(x,y) &= \max\left[0, K_y(x,y)\right]
\end{aligned} \tag{13}$$

it can be re-formulated via two different linear problem, as follows:

$$\min_{K_x K_y} \left\{ \sum_x \sum_y \begin{bmatrix} \left[c_x(x,y)K_x^+(x,y) + c_y(x,y)K_y^+(x,y)\right] \\ + \left[c_x(x,y)K_x^-(x,y) + c_y(x,y)K_y^-(x,y)\right] \end{bmatrix} \right\} \tag{14}$$

It can be seen that the problem stated in (14) can be transformed to define a minimum cost flow problem on a network (see Figure 2), with the new variables representing the net flow running along the network arcs. Once the network has been solved, the solutions in terms of the 2π-multiple integer functions will be expressed as follows:

$$\begin{aligned}
K_x(x,y) &= K_x^+(x,y) - K_x^-(x,y) \\
K_y(x,y) &= K_y^+(x,y) - K_y^-(x,y)
\end{aligned} \tag{15}$$

2.4 Extended Minimum Cost Flow (EMCF) algorithm

This section is focused on the presentation of the rationale at the base of the so-called Extended Minimum Cost Flow (EMCF) PhU technique that represents a way to efficiently incorporate temporal information in the phase unwrapping problem of sequence of multi-temporal differential interferograms. Before discussing the characteristics of the proposed

approach, some considerations about the MCF technique are first in order. The original minimum cost flow algorithm, thought to be applied to a regular spatial grid, was improved in order to deal with sparse data (Costantini, 1998). In particular, the grid of the investigated samples is typically chosen to be relevant to the coherent pixels present into the DInSAR interferograms, while the Delaunay triangulation is used to define the neighbouring points and the elementary cycles in the set of the identified coherent sparse pixels. The possibility to extend this approach to the three-dimensional case, in order to simultaneously unwrap an interferometric sequence, has already been investigated in (Costantini et. al., 2002). However, in this case, the problem cannot be formulated in terms of network minimum cost flow procedures. Accordingly, no computationally efficient codes are available and, therefore, the overall unwrapping process can be extremely time-consuming, particularly for long interferogram sequences.
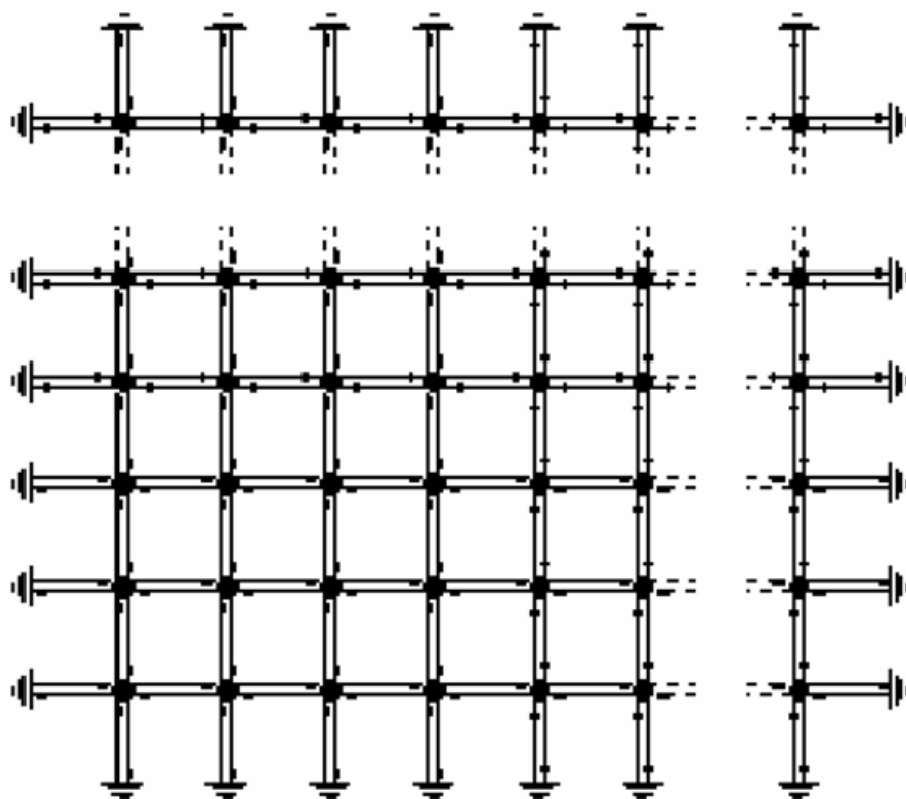

Fig. 2. A pictorial representation of the equivalent network to be solved for retrieving the 2π integer multiples needed to reconstruct a conservative phase field. The network nodes are associated to each residue-cut and the bidirectional arcs are related to the phase differences arcs.
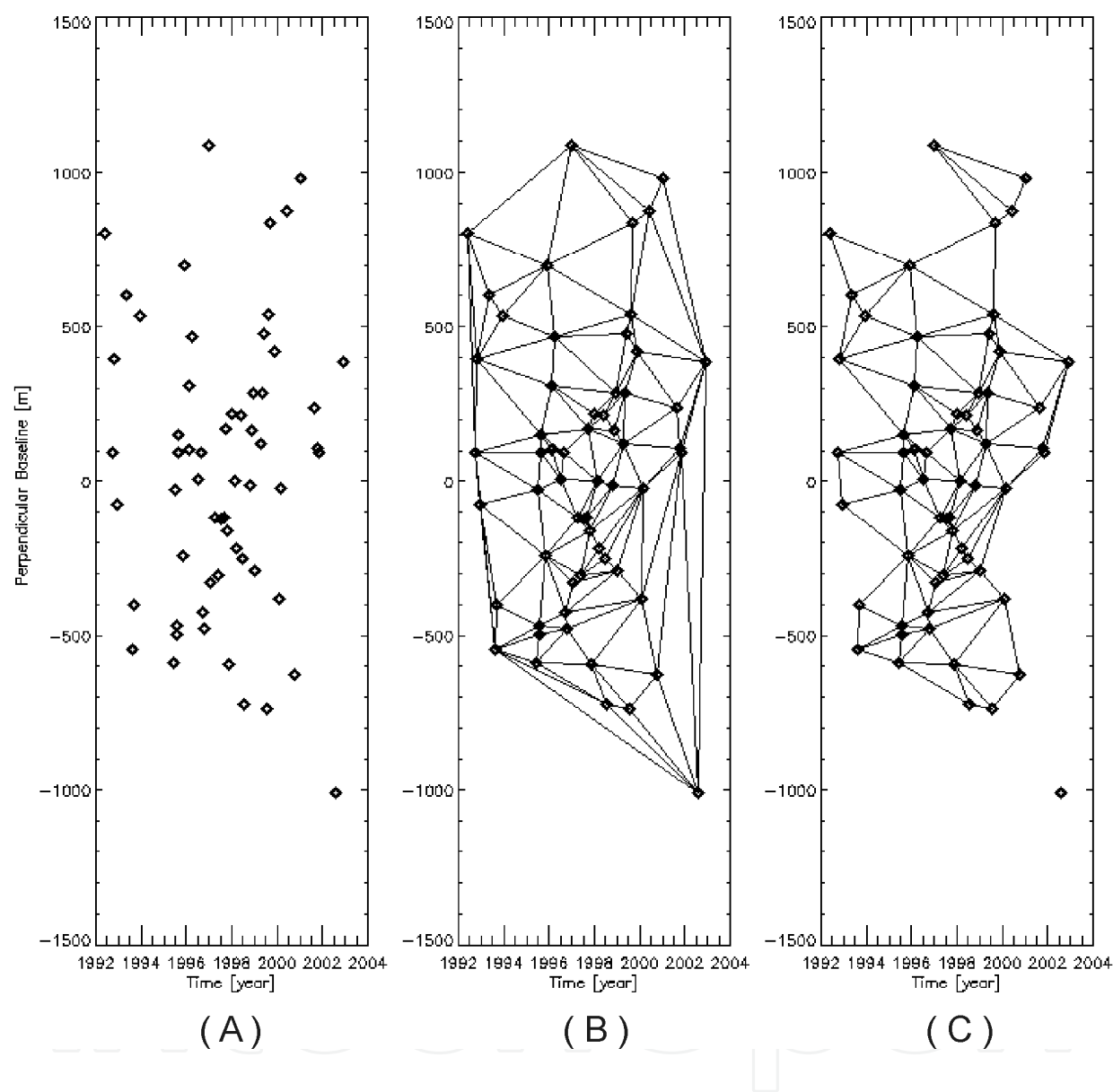
Fig. 3. SAR data representation in the temporal/perpendicular baseline plane for the ERS SAR data analyzed in the following experiments. (A) SAR image distribution. (B) Delaunay triangulation. (C) Triangulation after removal of triangles with sides characterized by spatial and/or temporal baseline values exceeding the selected thresholds (corresponding in our experiments to 300 m and 1500 days, respectively).

The proposed unwrapping solution, in addition to the spatial characteristics of each DInSAR interferogram, also exploits the temporal relationships among a properly selected interferogram sequence, thus allowing the performance improvement of the MCF technique.
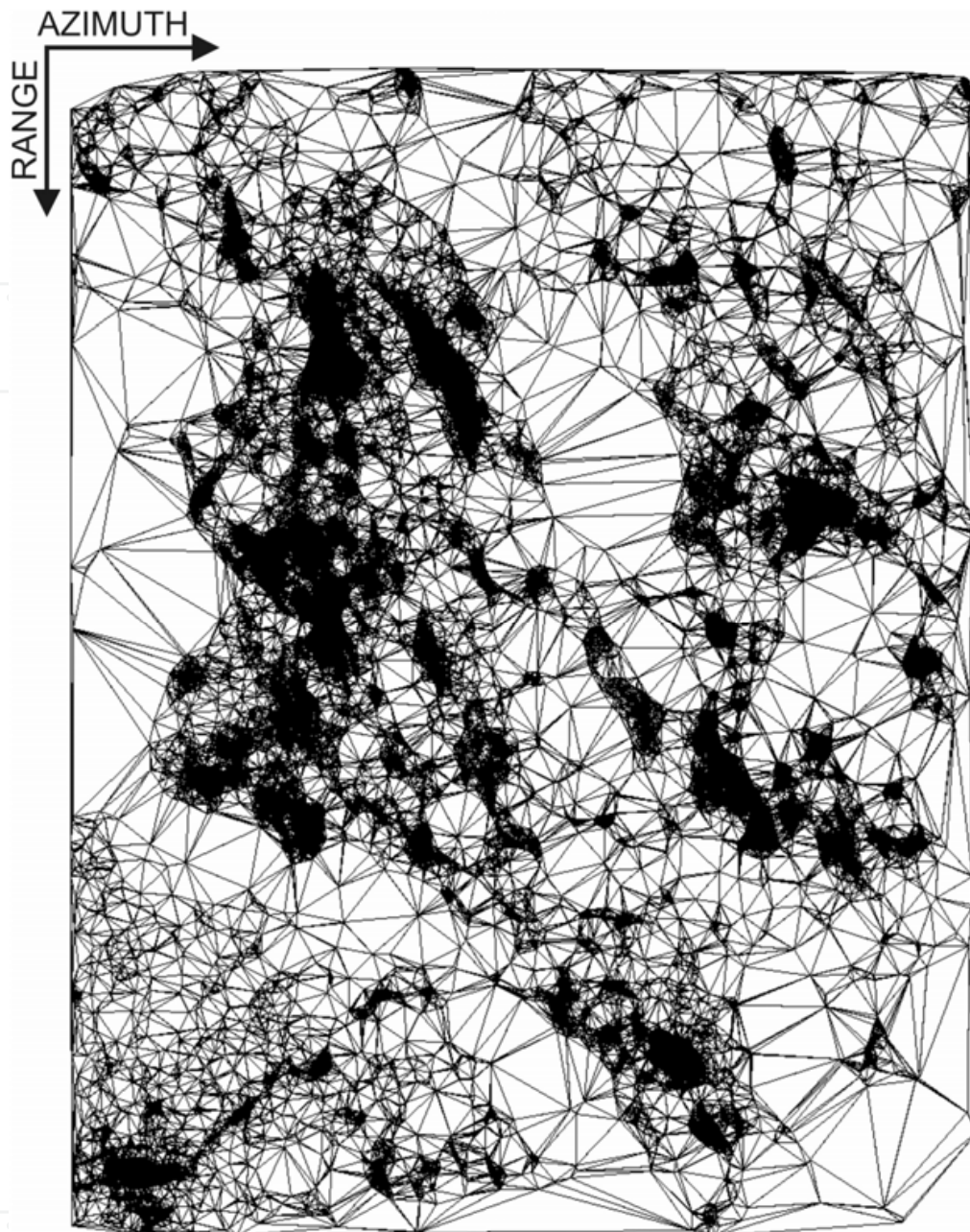
Fig. 4. Delaunay triangulation in the azimuth/range plane involving the set of spatially coherent pixels (in black).

The starting point of our approach, mostly oriented to deformation time-series generation, is the computation of two Delaunay triangulations. The former is relevant to the SAR data acquisitions distribution in the so-called "Temporal/Perpendicular baseline" plane and allows us to identify the DInSAR interferograms sequence to be computed; the latter is carried out in the Azimuth/Range plane and involves the coherent pixels common to the interferograms within the sequence. The unwrapping operation of the overall data set is then performed via a two-step processing procedure: first of all, we identify all the segments of the computed "spatial" triangles and, for each of these, we carry out a "temporal" PhU step by applying the MCF technique to the grid relevant to the temporal/perpendicular baseline plane. The second step uses, for each arc, the previously computed unwrapped

phases as a starting point for the subsequent spatial unwrapping operation, performed on each single interferogram; again the standard MCF network programming technique is applied and, in this case, we use the "costs" of the previous solutions to set the weights associated with the single arcs involved in the spatial unwrapping. Overall, the basic rationale of the procedure is quite simple: to exploit the temporal relationships among the computed multi-temporal interferograms to bootstrap the subsequent spatial unwrapping operation. We remark that the presented approach is focused on multilook interferograms. Moreover, the possibility to apply the MCF network programming algorithm to both the temporal and spatial unwrapping steps leads to a computationally efficient procedure. Let us start our analysis by investigating the generation process of the interferograms needed for the algorithm implementation discussed in the following sections. Accordingly, we consider a set of N+1 independent SAR images of the same area, which are co-registered with respect to a reference one, with respect to which we may compute the temporal and spatial (perpendicular) baseline components. Accordingly, each SAR image can be represented by a point in the temporal/perpendicular baseline plane (see Figure 3A) where we may also compute a Delaunay triangulation (see Figure 3B). Despite the constraints on the maximum allowed baseline extensions, we remark that the obtained triangulation may involve arcs relevant to data pairs whose baselines exceed the assumed maxima, thus potentially leading to generate interferograms strongly decorrelated. To avoid these effects without loosing our triangulation representation, we may remove all the triangles involving arcs with too large baselines, as shown in Figure 3C. Equivalently, we may also remove the triangles corresponding to interferograms including data pairs with large Doppler centroid differences; this is often the case for interferograms involving ERS data acquired after 2000, i.e., following the gyroscopes failure events (Miranda et. al., 2008). Notice that this triangles removal step may lead to discarding some acquisitions and/or to the generation of more than one independent subset of triangles, i.e., to a data representation consistent with the one described in the D-InSAR Small Baseline Subset (SBAS) procedure. Therefore, the compatibility between this data organization and the one exploited in the SBAS technique is clearly evident. Following the identification of the final triangulation, the computation of the DInSAR interferogram sequence is performed. At this stage, we can generate the "mask" of the pixels in the spatial plane that are considered coherent within the generated sequence. This mask can be obtained, for instance, by considering those pixels with an estimated coherence value greater than a selected threshold, which are common to a part or even to the entire interferogram sequence. Accordingly, as a final step, we compute a second Delaunay triangulation which involves the arcs connecting the neighbouring pixels of the computed mask.

The presented PhU procedure is based on a two-step processing approach that benefits of the information available from both the grids. In particular, the key idea is to carry out first, for each arc connecting neighbouring pixels, a "temporal" unwrapping operation which implies the basic MCF approach. The second step relies on the use of these results as a starting point for the "spatial" unwrapping performed on each single interferogram. The key issues of these two processing steps are described in the following analysis which is focused on the use of multilook interferograms. The temporal PhU method benefits from the relationships existing between the phase differences of pixel pairs relevant to the wrapped and unwrapped signals. In particular, if we consider the spatial arc connecting the generic A and B pixel pair in the spatial plane, the unknown, unwrapped phase difference can be expressed as follows

$$\Delta\tilde{\psi}_{AB} = \tilde{\psi}(A) - \tilde{\psi}(B) = \left\langle \tilde{\varphi}(A) - \tilde{\varphi}(B) \right\rangle_{-\pi,\pi} + 2\pi H_{AB} =$$
$$= \Delta\tilde{\varphi}_{AB} + 2\pi H_{AB}$$

(16)

Therefore, we may compute a Delaunay triangulation shown in Figure 4. In order to define a set of elementary cycles relevant to the coherent pixels only, and we may impose the irrotational property for the phase gradient, in a discrete space. At this stage, the PhU problem can be solved, as done for the original case, in a very efficient way by recognizing that a network structure underlines it and, by searching for the relevant network minimum cost flow solution, as fully described in (Pepe & Lanari, 2006). The unwrapped DInSAR phase differences computed via the previous temporal PhU step are then finally used as a starting point for the spatial unwrapping operation. This second step is carried out on the single interferograms through the application of the basic MCF unwrapping technique.

3. EMCF-based region growing technique

A different class of PhU algorithms is based on the general concept of the "region growing" allowing us to considerably increase the spatial density of the areas with correct unwrapped results. In particular, we present a space-time region growing (RG) technique whose core is represented by the EMCF algorithm described in section 2. Basic idea of such approaches is to retrieve the unwrapped phase of a set of investigated pixels that are in the neighbourhood of an already unwrapped region. In particular, the unwrapped phase of the analyzed pixels is computed by exploiting the phase values of neighbouring unwrapped points (Xu & Cumming, 1999). Notice that with respect to classic region growing approaches here we apply a method that allows to handle with non-linear deformation trends: this is beneficial to analyze areas characterized by strongly non-linear displacements behaviours. Some experimental results will be also presented to demonstrate the effectiveness of the proposed PhU methodology. In particular, the implemented RG-EMCF algorithm has been applied to sequences of multilook differential interferograms, relevant to the Central Nevada region, characterized by large non-linear deformation phenomena, as well as to a test site located in the Gardanne area (France), affected by strong decorrelation phenomena.

The method provides a prediction of the (unwrapped) phase values at a pixel in the neighborhood of a region of pixels that have already been unwrapped. Following the preliminary PhU operation, we identify two sets of pixels. The former consists of Q high quality points $\mathbf{S} = \left(S_0, S_1, ..., S_{Q-1} \right)$, hereinafter referred to as seed points, that are characterized by temporal coherence values greater than a given threshold (typically set to 0,7 for DInSAR analyses). Notice that the temporal coherence is a measure of the correctness of the obtained unwrapping results originally proposed in (Pepe & Lanari, 2006) that is not fully discussed here for the sake of brevity. The region-growing procedure starts by analyzing the candidate pixels in the proximity of the DInSAR reference point location, and proceeds along a path (for instance, a spiral) including all the previously selected candidate pixels.

For the sake of generalization, let us describe the *p-th* iteration of the algorithm, aimed at analyzing the multitemporal unwrapped phases at the generic candidate pixel C_p. This is done by exploiting the knowledge of the unwrapped phase values $\mathbf{\Psi}\left(S_{pi} \right)$ at the seed pixels S_{pi}, located within a rectangular area centered around the location of the candidate pixel [see Fig. 5(a)]. Thereby, we obtain different predictions of the (unwrapped) phases at the
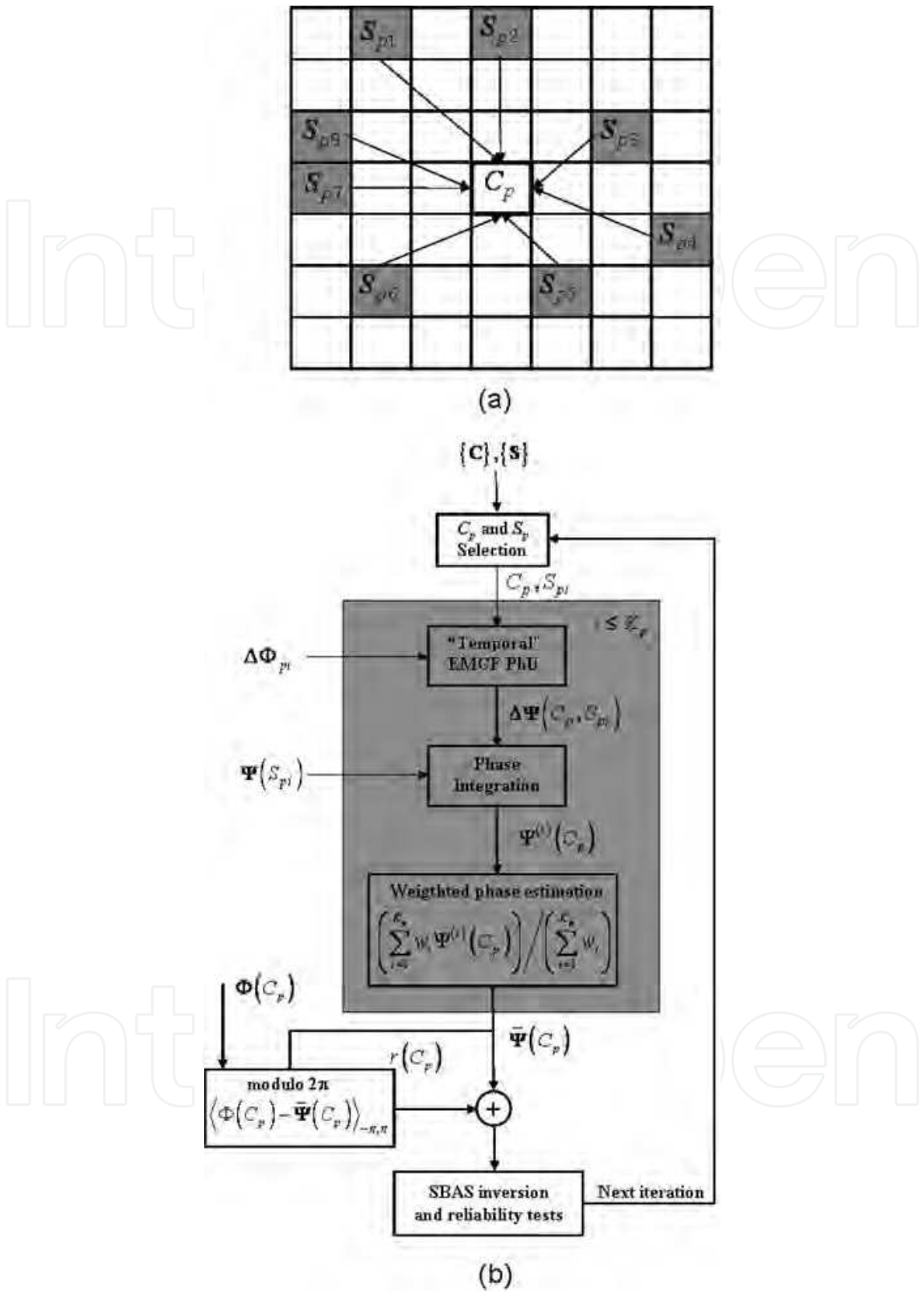
(a)

(b)

Fig. 5. EMCF-based region-growing algorithm. (a) Pictorial representation of the *p-th* iteration of the algorithm: the phase values at the candidate pixel (located at the center) are predicted by the phases of the eight-seed-pixels (gray boxes) located in its neighborhood. (b) Diagram block of the algorithm.

selected candidate pixel, namely $\mathbf{\Psi}^{(i)}\left(C_p\right)$, computed by integrating the phase differences along the paths connecting the candidate and the i-th seed pixel:

$$\mathbf{\Psi}^{(i)}\left(C_p\right) = \mathbf{\Psi}\left(S_{pi}\right) + \Delta\mathbf{\Psi}\left(C_p, S_{pi}\right) \quad i = 1, \ldots, K_p \tag{17}$$

where the estimate of the (unwrapped) phase difference $\Delta\mathbf{\Psi}\left(C_p, S_{pi}\right)$ over the given candidate/seed arc is retrieved by applying the temporal PhU strategy detailed in (Pepe & Lanari, 2006). However, since different integration paths lead to independent phase predictions at the candidate pixel, we carry out a weighted average of such individuals predictions:

$$\bar{\mathbf{\Psi}}\left(C_p\right) = \left(\sum_{i=1}^{K_p} w_i \Psi^{(i)}\left(C_p\right)\right) \Big/ \left(\sum_{i=1}^{K_p} w_i\right) \tag{18}$$

where the weights {w} are set taking into account the (achieved) temporal network minimum costs (Pepe & Lanari, 2006). The average prediction in (18) is eventually used to compute the (unwrapped) phase vector at the selected candidate pixel.

$$\mathbf{\Psi}\left(C_p\right) = \bar{\mathbf{\Psi}}\left(C_p\right) + \mathbf{r}\left(C_p\right) \quad i = 1, \ldots, K_p \tag{19}$$

where the $\mathbf{r}\left(C_p\right) = \left\langle \mathbf{\Phi}\left(C_p\right) - \bar{\mathbf{\Psi}}\left(C_p\right)\right\rangle_{-\pi,\pi}$ term on the right-hand side of (19) guarantees that unwrapped and wrapped phase vectors differ by 2π-integer multiples.

A check whether the prediction in (19) is correct is finally performed: if this is the case, the selected candidate pixel is added to the set of seed points, otherwise it is discarded from the following analyses. To the purpose, two different reliability tests are exploited.

Test 1- We invert (19) by the SBAS strategy and measure the related temporal coherence value (Pepe et al. 2006). The test is passed when the measured temporal coherence is greater than a given threshold.

Test 2- It relies on the assumption the larger the values of the residual phase vector the larger the probability to retrieve incorrect phase estimates. Accordingly, we analyze the residual phase dispersion through:

$$\Lambda\left(C_p\right) = \frac{\left|\sum_{k=0}^{M-1} \exp\left[jr\left(C_p\right)\right]\right|}{M} \tag{20}$$

This second test is passed when this additional coherence value is greater than a selected threshold.

The block diagram of the algorithm is sketched in Fig. 5b.

3.1 Real data results

In this section, we provide some experimental results relevant to two different test site areas (Casu, 2009): a wide area in central Nevada (USA) extending for about 600 x 100 km and the highly vegetated region of Gardanne (France).

The Central Nevada SAR data set consists of 264 ERS-1/2 SAR data frames (track 442, frames: from 2781 to 2871), spanning the 1992-2000 time interval, and we generate 148 multilook DInSAR interferograms, with a spatial resolution of about 160 x 160 m. Note that SAR data set and interferogram distribution are the same exploited by (Casu et al., 2008). First of all, we select the set of Seed Points from which the unwrapped phase will be propagated. To do this, we just impose a threshold value to the temporal coherence achieved by applying the EMCF algorithm, in particular we impose a value of 0.8, obtaining more than 850,000 Seed pixels. In Figure 6a it is shown the selected Seed Point mask.

In order to evaluate the phase unwrapping step performances, we compare the achieved RG-EMCF results with those obtained by using a conventional SBAS processing chain. In particular, Figure 6b and Figure 6c show the temporal coherence masks of the reliable pixels (obtained by imposing previous mentioned thresholds for the RG-EMCF algorithm and for the conventional one) relevant to the conventional and new Region-Growing algorithm, respectively. By a first qualitative analysis, it is clear that the RG-EMCF approach permits to obtain a larger number of points at a given coherence threshold. More systematically, we measured an increase of about 88% for the number of "grown" pixels, while the total image increment is of about the 32%.

Moreover, we also compute the temporal coherence histogram, shown in Figure 9, relevant to the common "grown" pixels only. It is clear the coherence improvement achieved by the RG-EMCF results. As mean coherence value we obtain 0.90 for the RG-EMCF approach while 0.85 for the conventional SBAS results. Also in this case, it is clearly visible the improvement of the new proposed algorithm.

As final remark, we present in Figure 7 the mean deformation velocity maps of the two sets of unwrapped phases processed via the SBAS approach. Figure 8 clearly demonstrates the RG-EMCF capability to increment reliable pixels not only in non deforming areas, but also in zone affected by strong and non linear deformation.

In general, Region-Growing is very helpful to unwrap wide areas. Indeed, to manage large set of points can imply PhU infeasibility, due to the complexity of the problem to be solved as well as to the high computational burden. Therefore, a cascade of global and local PhU steps permits to correctly unwrap large areas, by first deliberately reducing the amount of investigated points (Seed Pixels) and, subsequently, reconsidering the removed ones (Candidate Pixels) in a proper Region-Growing step.

However, a Region-Growing approach can be applied also in highly decorrelated region, where the low coherence implies to deal with a reduced amount of Seed Pixels. Therefore, a Region-Growing step can help increasing the unwrapped pixel spatial density.

Accordingly, we applied the proposed RG-EMCF PhU approach to the Gardanne (France) region which is highly vegetated and where an open pit mine is present. Therefore, the zone
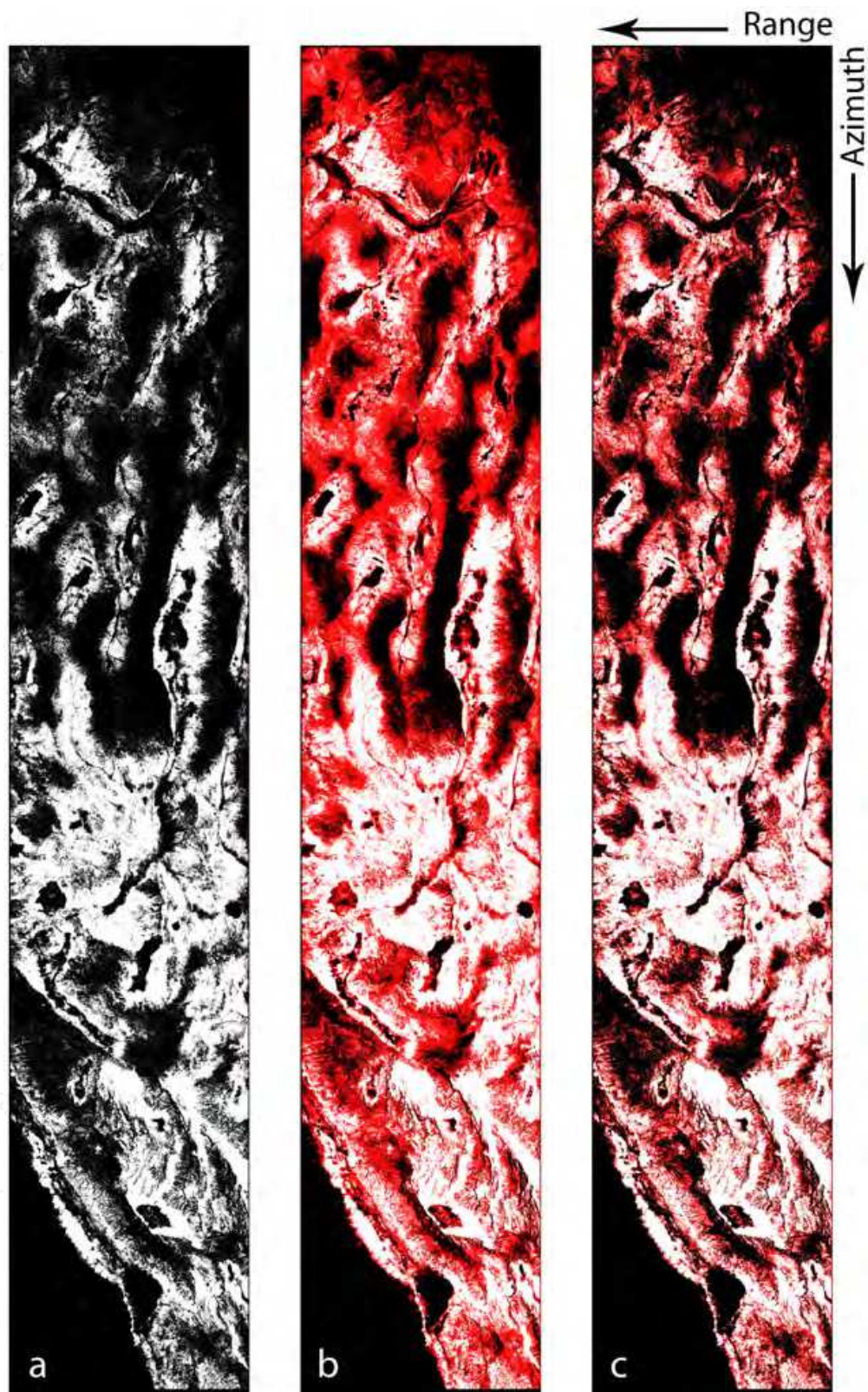
Fig. 6. Temporal coherence masks relevant to Central Nevada area. a) Seed Point mask (~850,000 pixels). b) RG-EMCF results (~1,770,000 pixels). c) Conventional SBAS results (~1,340,000 pixels). Grown points are highlighted in red while in white are represented the Seed Points of Figure 6a. By courtesy of dr. Francesco Casu (Casu, 2009).
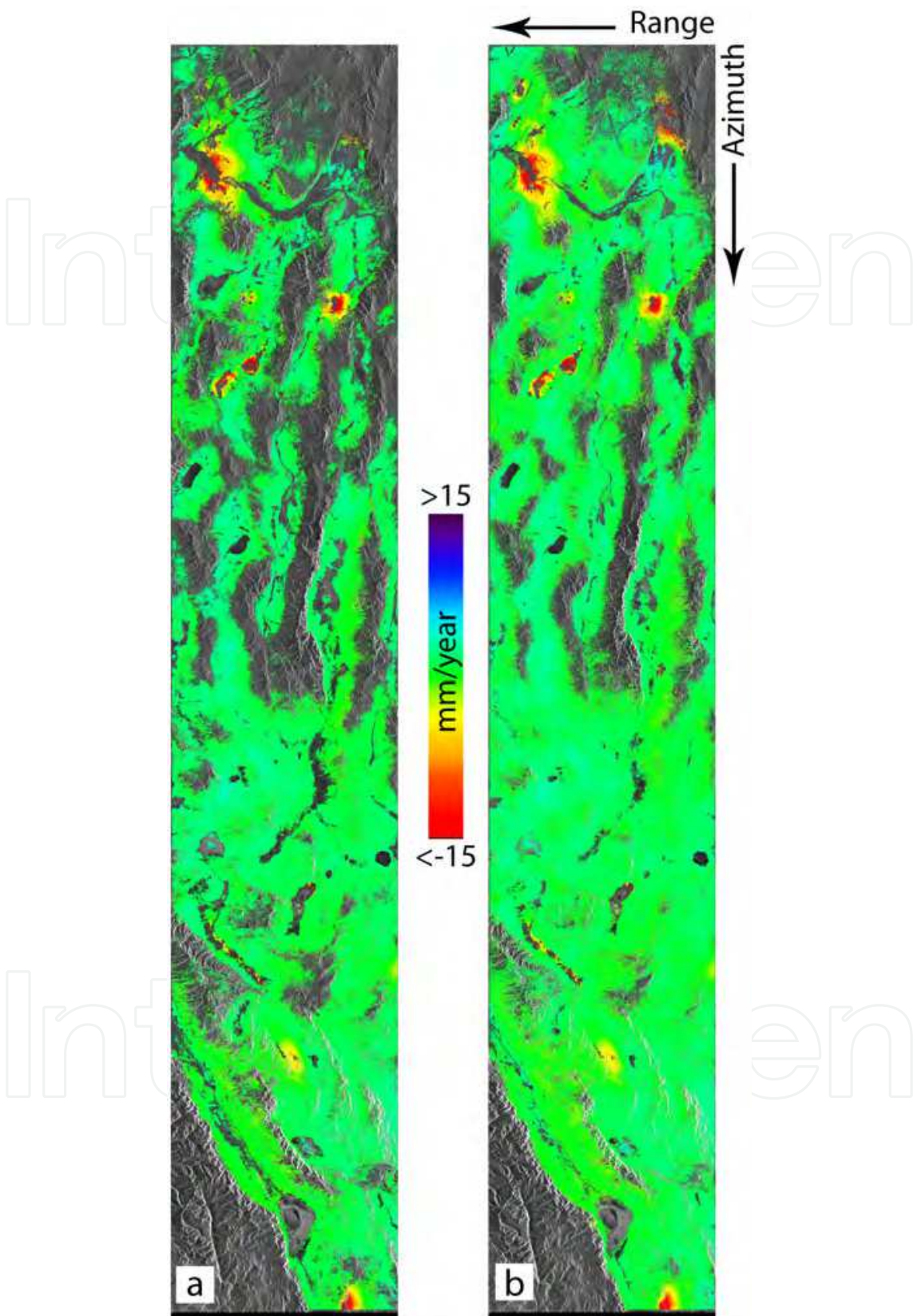
Fig. 7. Mean deformation velocity maps, in SAR coordinates, relevant to Central Nevada area. a) Conventional SBAS results. b) RG-EMCF results. By courtesy of dr. Francesco Casu (Casu, 2009).
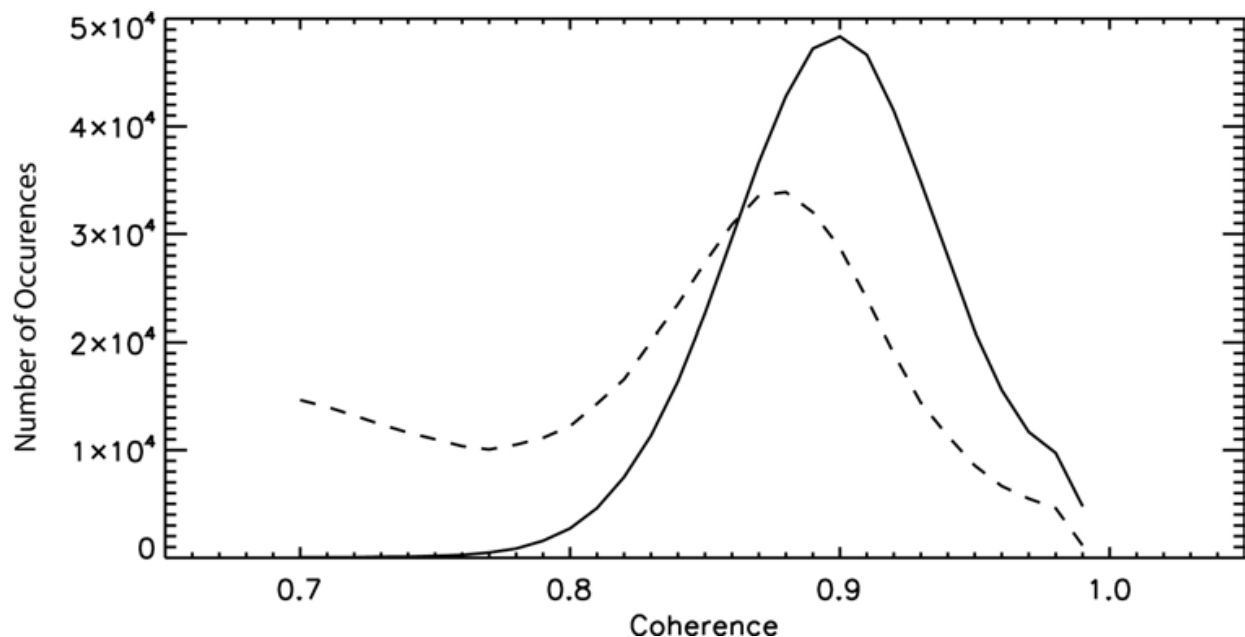
Fig. 8. Temporal coherence histogram relevant to common "grown" pixels obtained by exploiting conventional (dashed line) and new (continuous line) Region-Growing algorithm. By courtesy of dr. Francesco Casu (Casu, 2009).

is characterized by very low temporal coherence and is affected by strongly non linear deformation, implying to be a very critical test area for multi-temporal DInSAR analysis.

In Figure 9, we present the mean deformation velocity maps computed by applying the SBAS approach to a set of 75 ERS-1/2 and 8 ENVISAT images acquired in the 1992-2004 time period and coupled in 243 interferograms, the latter being unwrapped via both the procedure implemented in the SBAS processing chain and the RG-EMCF algorithm. Note that, DInSAR data have been multilook, obtaining a final spatial ground resolution of about 80 by 80 meters.

We just remark that, simultaneous exploitation of ERS and ENVISAT data implies that no cross sensor interferograms can be generated, due to the different signal wavelength of the two sensors. Therefore, the Temporal/Perpendicular baseline network will result decomposed in several subsets (at least two), corresponding to the different sensor interferograms. Also in this case, looking at Figure 9, it is clearly visible the strong increase of the correctly unwrapped pixels. Indeed, "grown" pixel number pass from about 2,500 for the conventional case to more than 87,000 for the RG-EMCF one, with a global improvement (for the whole area, i. e., accounting also for the Seed Points) of about the 113%. It is worthy to remark that the RG approach available in the SBAS processing essentially does not produced any results (only 2,500 "grown" pixels starting from 73,000 Seeds): this is because the strong decorrelation affecting the area.
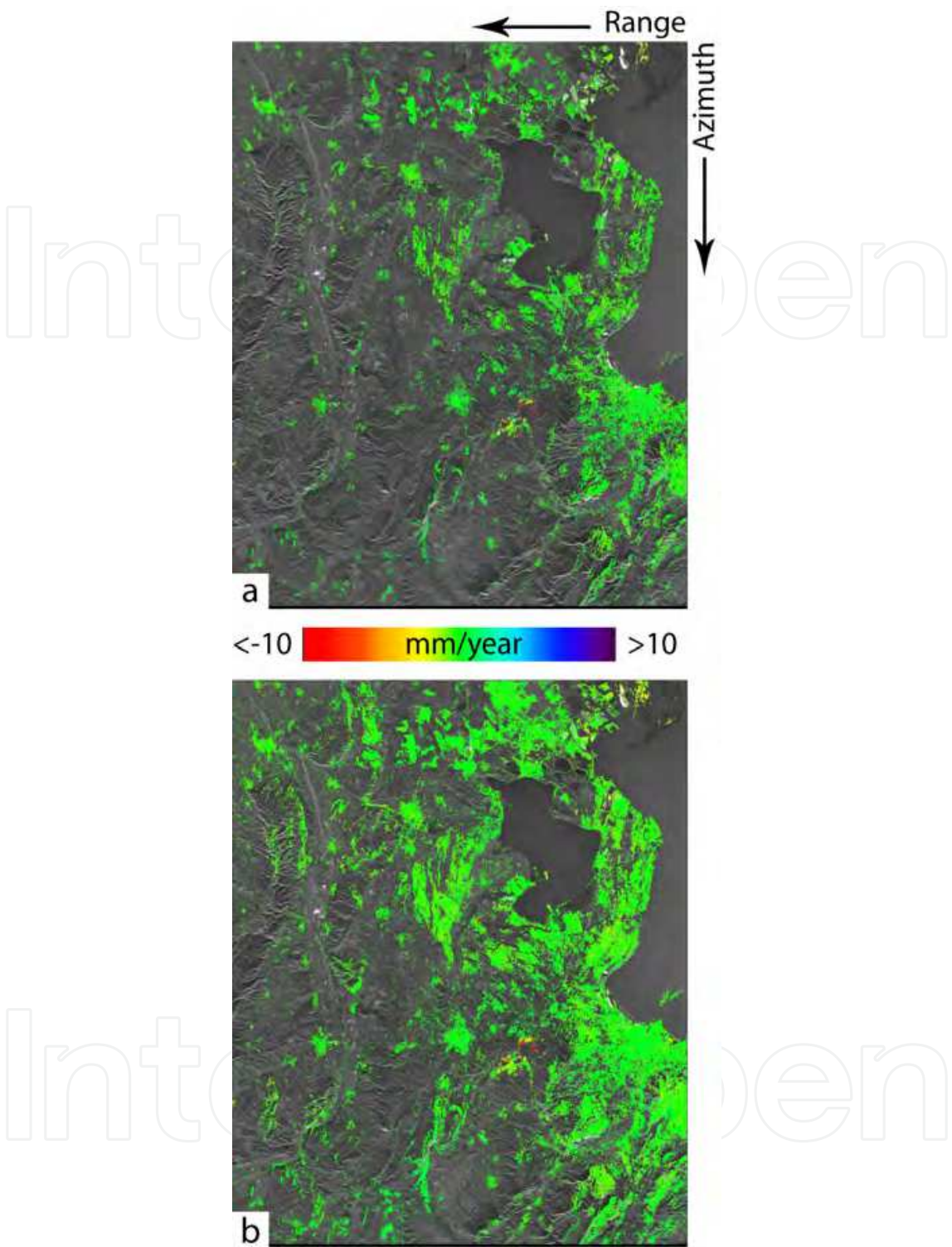
Fig. 9. Mean deformation velocity maps relevant to the Gardanne area (France). a) Conventional SBAS results. b) RG-EMCF results.

4. On unwrapping large interferograms

In this section, we propose to exploit the highly efficient EMCF algorithm as the core procedure to unwrap sequences of large single-look DInSAR interferograms suitable for the

generation of deformation time-series through the SBAS approach. This PhU approach allows us to directly apply the SBAS inversion to the unwrapped full resolution DInSAR phase sequences, with no need to pass through the analysis of the corresponding sequences of multi-look DInSAR interferograms (Lanari et. al., 2004). To properly solve this PhU problem, we suggest to apply an effective divide-and-conquer approach to the space-time phase unwrapping problem. The key idea is to divide the complex minimum cost flow network problems, implementing the whole PhU step, into that of simpler sub-networks, which are solved by applying the EMCF approach. More precisely, we start by identifying, and solving, a primary network that involves a selected set of very coherent pixels in our interferograms. The results of this primary network minimization, representing the backbone structure of the overall network, are subsequently used to constrain the solution of the remaining sub-networks, including the entire set of coherent pixels. To achieve this task, the second EMCF PhU step relies on the generation of a Constrained Delaunay Triangulation (CDT) (Chew, 1989), whose constrained edges are relevant to the set of successfully unwrapped pixels analyzed during the first PhU operation. We remark that our approach has some similarities with [6] where a two-scale strategy was also suggested to unwrap large interferograms; however our strategy is similar but inverted because in our scheme the primary PhU step is used to figure out a (global) PhU solution, and the secondary one to locally "propagate" the PhU solution in low coherent areas. The key idea of the proposed approach is to split our complex MCF network problem into that of simpler sub-networks. This solution can be efficiently implemented, as shown in the following, through two subsequent processing steps that are both carried out by using the EMCF technique.

Basically, the first PhU step is carried out on a set of very coherent pixels, used to compute a Delaunay triangulation in the Azimuth/Range plane, and the achieved PhU results are eventually exploited to successfully unwrap the remaining pixels. To achieve this task we solve a "constrained optimization problem" based on the computation of a Constrained Delaunay Triangulation (CDT) in the   plane from the grid of the overall coherent pixels. To clarify this issue, let us provide some basic information about the CDT, which is a triangulation of a given set of vertices with the following properties: 1) a pre-specified set of non-crossing edges (referred to as constraints, or constrained edges) is included in the triangulation, and (2) the triangulation is as close as possible to a Delaunay one. As an example, in Figure 10, it is shown a simple CDT relevant to a set of 96 points, see Fig. 10(a); in this case the selected constraints are represented by the 14 edges of the Delaunay triangulation generated from an eight-points subset of the originally 96 ones, see Fig. 10(b); the computed CDT is shown in Fig. 10(c), whereas the corresponding Delaunay triangulation is presented in Fig. 10(d).

Similarly to the case of Figure 10, we compute a CDT for the spatial grid of the coherent pixels , whose constrained edges are the arcs of the previously identified primary network. Since the EMCF Phase Unwrapping algorithm can work with generic triangular irregular grids, not necessarily Delaunay triangulations, it can be also applied to the irregular spatial grid obtained via our CDT. However, in this case we must solve a constrained optimization problem because we want to preserve, for each interferogram, the unwrapped phase values already obtained by solving the primary network. Accordingly, we perform the second unwrapping step again through the EMCF approach but applying the temporal PhU step only to the unconstrained arcs of the generated CDT. Moreover, the spatial PhU step is
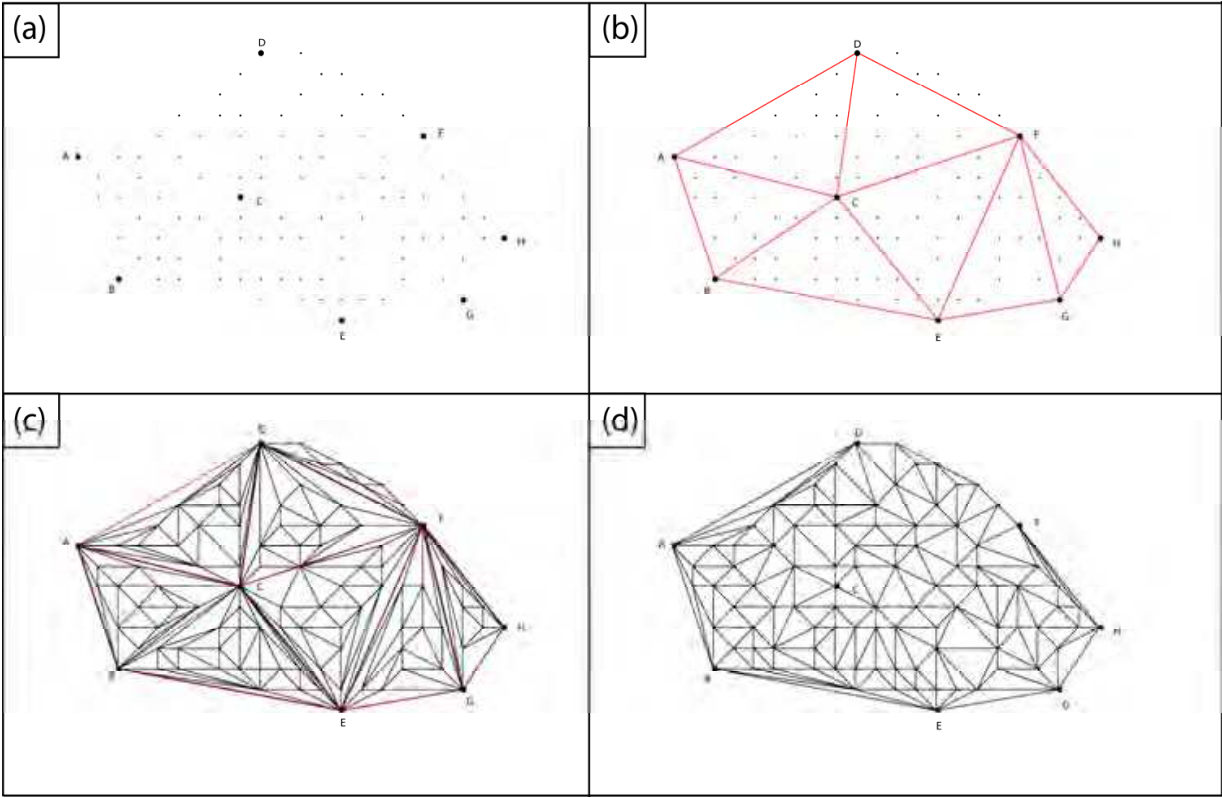
Fig. 10. Examples of Triangulations. (a) Dataset of 96 points with highlighted 8 of them, labeled to as A, B, C, D, E, F, G, H, respectively. (b) The 8-points Delaunay triangulation drawn with red lines (c) Constrained Delaunay Triangulation generated from the set of points of (a), and by using as constraints the triangulation of (b). (d) Delaunay triangulation computed from the 96 points in (a).

carried out on each single interferogram via the basic MCF approach but, in order to preserve the unwrapped phases relevant to the primary network, the weights used for the spatial MCF minimization must be properly set. If we refer to the generic PQ arc, this is easily achieved by imposing:

$$w_{PQ} = \begin{cases} L & PQ \in \{G_{Constrained}\} \\ 100 & \{PQ \notin \{G_{Constrained}\}\} \cap \{Cst_{min} < \rho\} \\ 1 & \{PQ \notin \{G_{Constrained}\}\} \cap \{Cst_{min} > \rho\} \end{cases} \tag{21}$$

where $\{G_{Constrained}\}$ is the set of constrained edges, and Cst_{min} is the temporal minimum network cost relevant to the given spatial arc. Moreover, L is a very large integer number, and ρ is a threshold value that is typically set not greater than 5% of the total number of interferograms. Based on (21), the flow into the constrained MCF network is automatically forced not to cross the constrained arcs and, as a consequence, the estimates of the primary network unwrapped phases are fully preserved. In other words, the presented approach allows us to effectively "propagate" the unwrapped solution from the primary network to the connected sub-networks, largely improving the phase unwrapping performances, and drastically decreasing the overall computational burden.
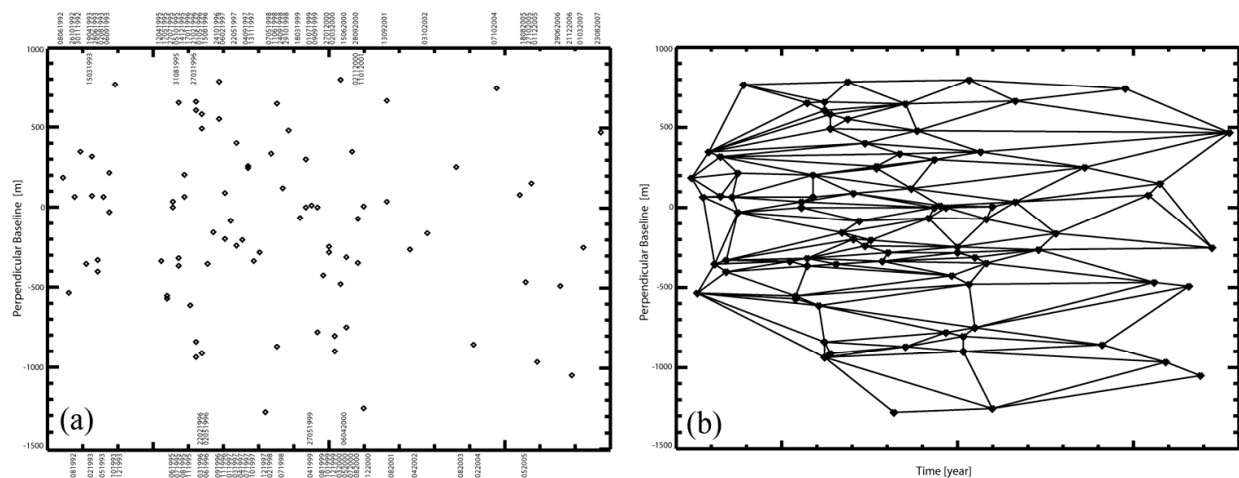
Fig. 11. SAR data representation in the temporal/perpendicular baseline plane for the ERS-1/2 SAR data analyzed in the following experiments, relevant to the Napoli (Italy) bay area. (a) SAR image distribution. (b) Delaunay Triangulation after the removal of triangles with sides characterized by spatial and temporal baseline values, as well as doppler centroid differences, exceeding the selected thresholds (corresponding in our experiments to 400 m, 1500 days and 1000 Hz, respectively).

The proposed approach was validated by analyzing a dataset of 86 ERS-1/2 SAR images acquired on descending orbits (Track 36, Frame 2781) between June 8, 1992 and August 23, 2007, over the Napoli (Italy) Bay area (see Figure 11). From these data, we identified a set of 234 data pairs characterized by perpendicular baseline values smaller than 400 m, and a maximum time interval of 1500 days. Precise satellite orbital information and a 3 arcsec SRTM DEM of the area were used to generate a sequence of single-look DInSAR interferograms. The computed interferograms were then unwrapped by applying the EMCF approach. To achieve this task, we first identified the spatial grid of all the coherent pixels to be unwrapped, composed of about 530 000 pixels, where 50 000 of them are very coherent. From the latter pixels, we generated, in the spatial plane, a Delaunay triangulation. The arcs of this triangulation represent the constrained edges of the implemented CDT: this structure connects the overall set of coherent pixels , and is essential for the second EMCF PhU step, leading to the final estimate of the unwrapped interferograms on the chosen spatial grid.

Figure 12 shows a false color map of the detected mean deformation velocity, where only points with high data quality are included, superimposed on a multi-look SAR amplitude image of the area. Moreover, in order to further investigate the achieved accuracy of the proposed approach, we focused on the Napoli city and surroundings, including Campi Flegrei caldera [see Fig. 3(a)] where independent geodetic information (leveling and GPS measurements) was available. In particular, for our analysis, we considered pixels located in correspondence to continuous GPS stations and leveling benchmarks and, for each of these points, we compared the retrieved DInSAR time-series with those obtained from the geodetic measurements, projected on the radar LOS. Note that, although we did not perform any filtering of the atmospheric phase artifacts affecting the DInSAR time-series, there is a good agreement between the SAR and the geodetic measurements. These results f confirm the effectiveness of the proposed phase unwrapping approach.
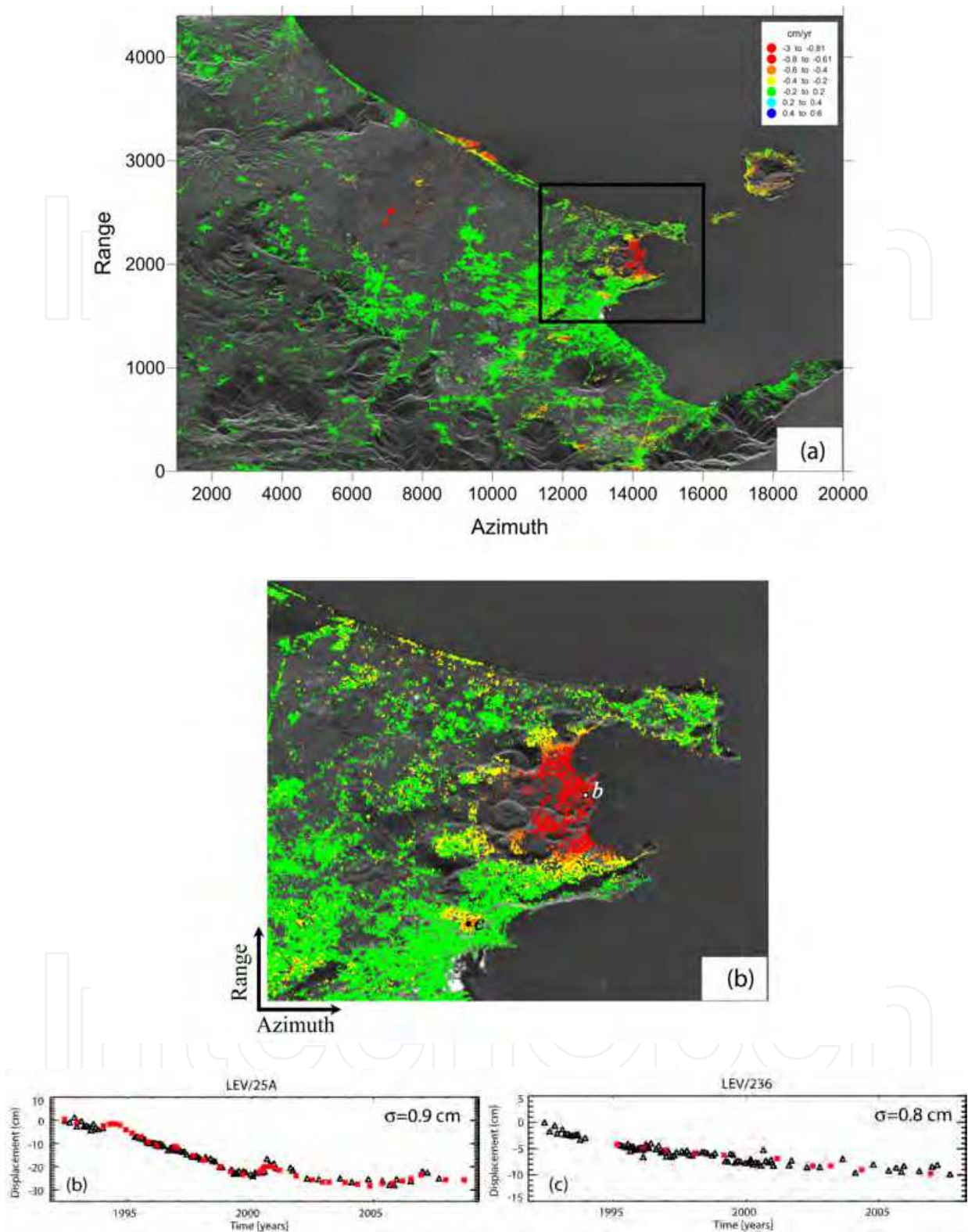
Fig. 12. ERS-1/2 DInSAR results. (a) Geocoded map of the mean deformation velocity of the investigated area (b) Zoomed view of the area of Napoli city and Campi Flegrei caldera (Italy) highlighted by the black box in (a). The plots show the DInSAR/leveling comparison of the deformation time-series corresponding to the pixels in (a) labeled as b (25A leveling benchmark) and c (236 leveling benchmark), respectively.

5. Conclusion

This chapter has presented a short review of some advanced multi-temporal phase unwrapping approaches for the generation of surface deformation time series through the application of the Small Baseline Subset (SBAS) DInSAR technique. Following a description of the basic rationale of the PhU problem, we have described in details the space-time PhU algorithm known as Extended Minimum Cost-Flow (EMCF). Finally, we focused on the recent improvements of this algorithm to analyze large interferograms affected by significant decorrelation effects and/or with severe non-linear deformation signals. The presented results clearly demonstrate the validity of these approaches and their valuable applicability in real cases.

6. Acknowledgment

7. References

D. Massonnet, and K. L. Feigl, "Radar Interferometry and its application to changes in the earth's surface," Rev. of Geophys., vol. 36, no. 4, pp. 441–500, doi:10.1029/97RG03139, 1998.

R. Bürgmann, P. A. Rosen, and E. J. Fielding, "Synthetic aperture radar interferometry to measure Earth's surface topography and its deformation," Annual Review Earth Planet Science, vol. 28, pp. 169–209, May 2000.

A. K. Gabriel, R. M. Goldstein, and H. A. Zebker, "Mapping small elevation changes over large areas: Differential interferometry," J. of Geophys. Res., vol. 94, no. B7, pp. 9183–9191, March 1989.

D. Massonnet, M. Rossi, C. Carmona, F. Adragna, G. Peltzer, K. Feigl, and T. Rabaute, "The displacement field of the Landers earthquake mapped by radar interferometry," Nature, vol. 364, no. 6433, pp. 138–142, Jul. 1993.

R. M. Goldstein, H. Engelhardt, B. Kamb, and R. M. Frolich, "Satellite radar interferometry for monitoring ice sheet motion: Application to an antarctic ice stream," Science, vol. 262, no. 5139, pp. 1525–1530, Dec. 1993.

D. Massonnet, P. Briole, and A. Arnaud, "Deflation of Mount Etna monitored by spaceborne radar interferometry," Nature, vol. 375, no. 6532, pp. 567–570, Jun. 1995.

G. Peltzer, and P. A. Rosen, "Surface displacement of the 17 May 1993 Eureka Valley earhtquake observed by SAR interferometry," Science, vol. 268, no. 5215, pp. 1333-1336, Jun. 1995.

A. Ferretti, C. Prati, and F. Rocca, "Permanent scatterers in SAR interferometry," IEEE Trans. Geosci. Remote Sens., vol. 39, no.1, pp. 8-20, Jan. 2001.

P. Berardino, G. Fornaro, R. Lanari, and E. Sansosti, "A new algorithm for surface deformation monitoring based on small baseline differential SAR interferograms," IEEE Trans. Geosci. Remote Sens., vol. 40, no. 11, pp. 2375–2383, Nov. 2002.

A. Hooper, H. Zebker, P. Segall, and B. Kampes, "A new method for measuring deformation on volcanoes and other natural terrains using InSAR persistent scatterers," Geophys. Res. Lett., vol. 31, L23611, doi:10.1029/2004GL021737, Dec. 2004.

O. Mora, J. J. Mallorquí, and A. Broquetas, "Linear and nonlinear terrain deformation maps from a reduced set of interferometric SAR images," IEEE Trans. Geosci. Remote Sens., vol. 41, pp. 2243–2253, Oct. 2003.

H. A. Zebker and J. Villasenor, "Decorrelation in interferometric radar echoes," IEEE Trans. Geosci. Remote Sens., vol. 30, no. 5, pp. 950–959, Sep. 1992.

R. Lanari, O. Mora, M. Manunta, J. J. Mallorquì, P. Berardino, and E. Sansosti, "A Small Baseline Approach for Investigating Deformation on Full resolution Differential SAR Interferograms," IEEE Trans. Geosci Remote Sens., vol. 42, no. 7, Jul. 2004.

H. A. Zebker and Y. Lu "Phase Unwrapping Algorithms for radar interferometry: residue-cut, least-squares, and synthesis algorithm J. Opt Soc. Am A. 15, 586-598, 1998;

R. M. Goldstein, H. A. Zebker and C. L. Werner: "Satellite radar interferometry: two-dimensional phase unwrapping", Radio Sci., 23, 1988;

D. C. Ghiglia and L. A. Romero: "Robust two-dimensional weighted and unweighted phase unwrapping that uses fast transform and iterative methods", J. Opt. Soc. Am. A, 11, 1994;

G. Fornaro, G. Franceschetti, R. Lanari, E. Sansosti: "Robust phaseunwrapping techniques: a comparison", J. Opt. Soc. Am A., 13, 2355,1996;

M. Costantini: "A novel phase unwrapping method based on network programming", IEEE vol 36, 3 May 1998, pp 813-821;

M. Costantini, F. Malvarosa, F. Minati, L. Pietranera and G. Milillo, "A Three-dimensional Phase Unwrapping Algorithm for Processing of Multitemporal SAR Interferometric Measurements," in Proc. Geosc, and Rem. Sensing Symposium, Toronto (Canada), 2002, vol. 3, pp. 1741-1743.

N. Miranda, B. Rosich, C. Santella, and M. Grion: "Review of the impact of ERS-2 piloting modes on the SAR Doppler stability", in Proc. Fringe,Frascati, Italy, Dec. 2003, CD-ROM;

A. Pepe, and R. Lanari R., "On the extension of the minimum cost flow algorithm for phase unwrapping of multitemporal differential SAR interferograms," IEEE Trans. Geosci. Remote Sens., vol. 44, no. 9, pp. 2374-2383, Sept. 2006.

W. Ku, and I. Cumming, "A Region-Growing Algorithm for InSAR Phase Unwrapping, " IEEE Trans. Geosci. Remote Sens., vol. 37, pp. 124–134, Jan. 1999

F. Casu, "The Small BAseline Subset technique: performance assessment and new developments for surface deformation analysis of very extended areas", PhD thesis, 2009

F. Casu, M. Manzo, A. Pepe, and R. Lanari, "SBAS-DInSAR Analysis of Very Extended
    Areas: First Results on a 60000-km2 Test Site," IEEE Geosci. and Remote Sensing
    Lett., vol. 5, no. 3, pp. 438-442, Jul. 2008.
L. P. Chew, "Constrained Delaunay triangulations," in Algorithmica, vol. 4, Springer.
    Verlag. New York 1989, pp. 97–108.
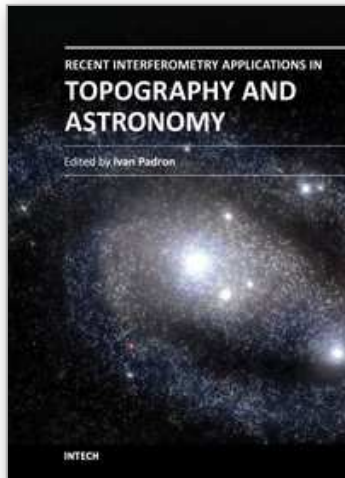
Recent Interferometry Applications in Topography and Astronomy

Edited by Dr Ivan Padron

ISBN 978-953-51-0404-9

Hard cover, 220 pages

Publisher InTech

Published online 21, March, 2012

Published in print edition March, 2012

This book provides a current overview of the theoretical and experimental aspects of some interferometry techniques applied to Topography and Astronomy. The first two chapters comprise interferometry techniques used for precise measurement of surface topography in engineering applications; while chapters three through eight are dedicated to interferometry applications related to Earth's topography. The last chapter is an application of interferometry in Astronomy, directed specifically to detection of planets outside our solar system. Each chapter offers an opportunity to expand the knowledge about interferometry techniques and encourage researchers in development of new interferometry applications.

How to reference

In order to correctly reference this scholarly work, feel free to copy and paste the following:

Antonio Pepe (2012). Advanced Multitemporal Phase Unwrapping Techniques for DInSAR Analyses, Recent Interferometry Applications in Topography and Astronomy, Dr Ivan Padron (Ed.), ISBN: 978-953-51-0404-9, InTech, Available from: http://www.intechopen.com/books/recent-interferometry-applications-in-topography-and-astronomy/advanced-multitemporal-phase-unwrapping-techniques-for-differential-synthetic-aperture-radar-dinsar-